Korean J. Chem. Eng., 37(5), 743-754 (2020)
DOI: 10.1007/s11814-020-0498-1

pISSN: 0256-1115
eISSN: 1975-7220

Design of vortex finder structure for decreasing the pressure drop of a cyclone separator

Yaquan Sun*, Junzhi Yu*,,†, Weibing Wang*,†, Shanglin Yang*, Xue Hu*, and Jingan Feng***

*Department of Mechanical and Electrical Engineering, Shihezi University, Shihezi 832000, China
**State Key Laboratory for Turbulence and Complex Systems, Department of Mechanics and Engineering Science, BIC-ESAT, College of Engineering, Peking University, Beijing 100871, China
(*Received 16 August 2019 • accepted 29 January 2020*)

Abstract−The structure of the vortex finder has an important influence on the pressure drop and separation efficiency of a cyclone, which mainly governs the separation process. In this paper, the traditional vortex finder is slotted on side wall and its bottom is closed, i.e., a slotted vortex finder. The impact of slotted vortex finder on the separation performance of a cyclone is explored by using numerical simulation and experimental validation. Specifically, the gas phase is studied by the Reynolds stress model (RSM), and the particle phase is simulated by the discrete phase model (DPM). The simulation results are in good agreement with the experimental results, revealing higher prediction accuracy. The results indicate that the slotted vortex finder can effectively suppress the generation of the downward swirling flow at the center of the vortex finder and decrease the turbulence intensity at the bottom of the vortex finder and the outer vortex, thereby decreasing the energy loss and increasing the separation efficiency. When the slot length is 0.2De, the slotted vortex finder can reduce the pressure drop by 143.33 Pa while increasing the collection efficiency by 5.51%.

Keywords: Slotted Vortex Finder, Cyclone Separator, Pressure Drop, Particle Trajectory, Turbulence Intensity, Separation Efficiency

INTRODUCTION

Gas cyclones have been widely used as gas-cleaning apparatus in chemical engineering, environmental cleaning, mineral processing and other industrial fields due to their low manufacturing cost, low power consumption, simple construction, and high separation efficiency [1]. The main purpose of the gas cyclone is to remove the solid dust carried in the gas as much as possible. A cyclone separator is generally composed of two outlets, a vortex finder, a cylindrical part, a conical part, and a dust collector [2]. As a crucial part of a gas cyclone, the vortex finder has an important influence on the gas-solid collection performance of the separator [3-5].

At present, analyzing the complicated three-dimensional (3D) gas-solid flow pattern into gas cyclones is an important concern. With increasing computational power, computational fluid dynamics (CFD) is applied to analyze various cyclones [6-8]. Based on three turbulence closure models, a cyclone separator was analyzed by Hoekstra et al. [9]. According to their results, the RSM turbulence model is consistent with the experimental results, whilst the other turbulence models predict an unrealistic contour of tangential and radial speeds. Slack et al. [10] evaluated the gas-solid flow field in a traditional high-efficiency gas cyclone by using the RSM and reported reasonable agreement between the RSM results and the experimental results. Using the RSM turbulence methodology, Wang et al. [11] compared the numerical performance and the experimental results of gas-oil cyclone separators, and found that the numerical performance is consistent with the experimental performance and the RSM is reliable for gas-oil cyclones.

To enhance the separation performance of gas cyclones, many researchers have studied the structure and diferent operating conditions of gas cyclones, and made certain scientific achievements. Li et al. [12] analyzed a guide-vane-inlet cyclone with a new vortex finder using the experimental approach. The results demonstrated that the new vortex finder can improve the performance of the guide-vane-inlet separator, as well as remove the particles with diameter more than 4 μm. Hesham et al. [13] also analyzed cyclones with various lengths or radius of vortex finders, and reported that the changes in the vortex finder radius can increase or decrease the energy loss. When the ratio of the vortex finder radius to the cyclone cylinder radius is between 0.3 and 0.7, the cyclone separator has the best performance. Chen and Liu [14] showed superiority of cyclones with a modified vortex finder under various contracting angles and sloping angles in increasing separation efficiency over other modifications. The best separation performance was obtained by the cyclone modified by the contracting angle of 30°. Later, Khairy [15] and Brar [16] demonstrated dramatic improvement in the separation efficiency by reducing the radius of the vortex finder, while aggravating the instability of the swirl flow. Zhu and Lee [17] identified the collection performance of gas cyclones under seven different vortex finder lengths, concluding that the length and insertion depth of the vortex finder have important influences on the collection performance. Rafiee et al. [18] analyzed the convergent vortex tube (VT) cyclone separator with different geometrical and operational parameters (throttle angle, injection slot number, and opera-

†To whom correspondence should be addressed.
E-mail: wwbshz@163.com, junzhi.yu@ia.ac.cn

tional pressure) by experimental study and CFD analysis. They optimized the parameter values so as to obtain the best separation, cooling, and heating performances. Gao et al. [19] optimized the lengths and radius of the vortex finder for decreasing total energy loss by using the RSM. Their findings reported that reducing vortex finder radius can slightly decrease the overall energy loss and the tangential velocity of the gas flow. Parvaz et al. [20] showed that the deviation of vortex finder can increase the energy loss while decreasing the collection efficiency. As the deviation of the vortex finder increases, the tangential velocity of the stream field is increased. Instead of conventional vortex finder, Pei et al. [21] designed a gas cyclone with inserted metal sheets in the vortex finder. In their study, the metal sheets can either lead to the disappearance of the backflow in the vortex finder or increase the collection efficiency due to the increase of turbulence intensity in the outer free vortex. Rafiee et al. [22] explored the effect of different operating fluids on the separator performance by analyzing the separation process in a Ranque-Hilsch vortex tube cleaning (cooling) system. The results showed that nitrogen dioxide creates the greatest separation power in comparison with the use of other gases.

According to the priorly reported scientific works, many researchers have succeeded in optimizing the sizes and shapes of vortex finders to improve the performance of cyclone separators. However, up to now, few researchers have focused on how to reduce the large amount of energy loss caused by the high swirling velocity of the gas flow in the vortex finder. Therefore, our purpose was to design a separator with a slotted vortex finder, which can decrease the energy loss in the vortex finder and hence decrease the overall pressure drop and improve the collection performance. Unlike the traditional vortex finder, the bottom of the slotted vortex finder is closed and it is slotted on side wall. The slots have different lengths and widths. We mainly focused on the effects of the slotted vortex finder on the gas-solid flow and performance of a separator. The gas phase and the particle phase of modified cyclones were simulated by the RSM model and the DPM model, respectively.

EXPERIMENTAL APPARATUS

To compare the collection performance and flow pattern of the modified cyclones with the traditional separator, a traditional separator which has the same cyclone structure was also constructed.

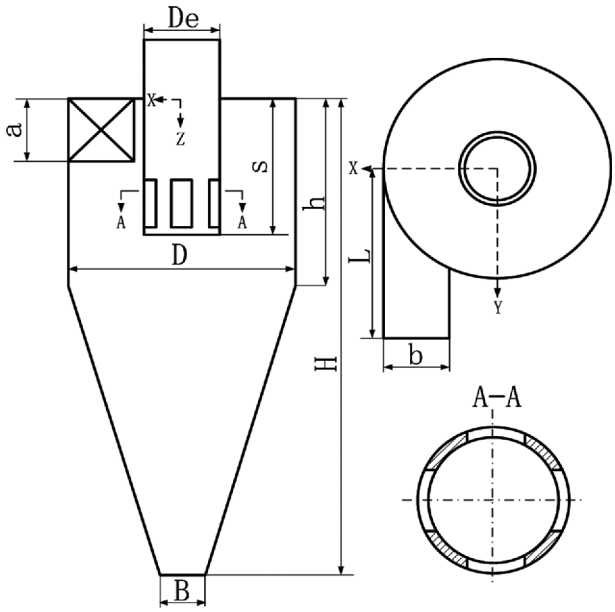

Fig. 1. Geometry of the cyclone and coordinate definition.

Table 1. Dimensions of the cyclone

Dimension	Symbol	Length (mm)
Body diameter	D	150
Inlet height	a	50
Inlet width	b	50
Diameter of the vortex finder	De	50
Height of the vortex finder	s	88
Cyclone body height	h	128
Cyclone height	H	326
Cone-tip diameter	B	3

The sizes and coordinates of the gas separator are shown in Fig. 1 and Table 1.

Specifically, Fig. 1 illustrates the bottom of the slotted vortex finder is closed and there are four rectangular slots on the low part of the side wall. For the impact of slot length and width, six cases were studied, including 0.2De, 0.3De, 0.4De, 0.5De, 0.6De, respectively.

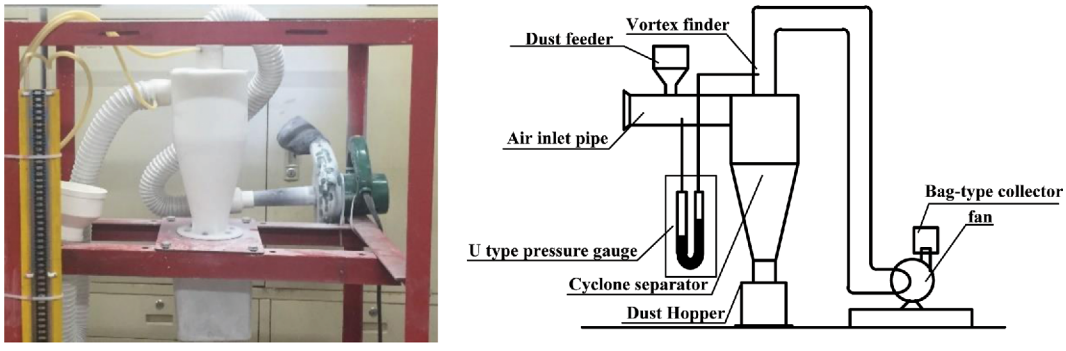

(a) (b)

Fig. 2. (a) A photo of the experimental system; (b) schematic representation of experimental setup.

Table 2. Particle diameter distribution of calcium carbide slag

Particle diameter/μm	0-2.5	2.5-5	5-7.5	7.5-10	10-12.5	12.5-15
Content/%	5.6	10.6	16.4	20.1	21.6	25.7
Grand total/%	100.0	94.4	83.8	67.4	47.3	25.7

As shown in Fig. 2, the experimental system is a circulation loop mainly composed of a cyclone separator, an air inlet pipe, a dust hopper, a vortex finder and a fan. The inlet measurement point of pressure drop is set at the inlet, the outlet measurement point is set at the outlet of the exhaust pipe, and the experiment was performed at normal temperature. Calcium carbide slag after grinding was used as the experimental solid particles with a physical density of 2,234 kg/m^3. A laser particle size analyzer (range 0.2 μm to 500 μm with an accuracy of ±3%) was used to measure the particle diameter distribution of the calcium carbide slag particles, and the data are listed in Table 2.

During the experiment, first, the air was pumped into the empty separator by a fan, and the motor speed of the fan was regulated by the frequency converter to control the inlet air velocity to be 17 m/s. After 2 minutes, the mass ratio of the particles collected by the dust hopper to the particles added to the inlet was calculated by electronic scale (range 0.001 g to 150 g with an accuracy of ±1%), and the total efficiency of the separator was obtained. In particular, a U-type pressure gauge (range 0 pa to 2,000 pa with an accuracy of ±1%) was used to obtain the pressure drop.

NUMERICAL SETUP

1. Turbulence Modeling

When the Fluent software is applied to study the flow pattern in a gas separator, the commonly used turbulence models include the RSM turbulence model, the RNG k-ε model and the standard k-ε model [9]. RSM model is the most elaborate type of RANS turbulence model that FLUENT provides. Abandoning the isotropic eddy-viscosity hypothesis, the RSM closes the Reynolds-averaged Navier-Stokes equations by solving transport equations for the Reynolds stresses, together with an equation for the dissipation rate. Besides, since the RSM accounts for the effects of streamline curvature, swirl, rotation, and rapid changes in strain rate in a more rigorous manner than one-equation and two-equation models. Compared with the other two models, it has greater potential to give accurate prediction for the highly swirling flows in cyclones. The governing equation of the RSM is described as follows [22]:

$$\frac{\partial(\overline{u_i'u_j'})}{\partial t}+\frac{\partial(U_k\overline{u_i'u_j'})}{\partial x_k}=D_{T,ij}+D_{L,ij}+P_{ij}+j_{ij}+e_{ij} \tag{1}$$

where, the turbulent diffusive term $D_{T,ij}$ can be written as

$$D_{T,ij}=-\frac{\partial}{\partial x_k}\left(\overline{u_i'u_j'u_k'}+\frac{\overline{p'u_j'}}{r}d_{ik}+\frac{\overline{p'u_i'}}{r}d_{jk}\right). \tag{2}$$

The molecular diffusive transport $D_{L,ij}$ is described as

$$D_{L,ij}=-\frac{\partial}{\partial_{x_k}}\left(\frac{\nu_t}{\sigma_k}\frac{\partial\overline{u_i'u_j'}}{\partial x_k}\right). \tag{3}$$

The stress generation term P_{ij} is given as

$$P_{ij}=-\left(\overline{u_i'u_k'}\frac{\partial u_j}{\partial_{x_k}}+\overline{u_i'u_k'}\frac{\partial u_j}{\partial_{x_k}}\right). \tag{4}$$

The pressure strain correlation term φ_{ij} is given as

$$\varphi_{ij}=\frac{p'}{\rho}\left(\overline{\frac{\partial u_i'}{\partial x_j}}+\overline{\frac{\partial u_j'}{\partial x_i}}\right). \tag{5}$$

The dissipation term ε_{ij} is given as

$$\varepsilon_{ij}=2\nu\overline{\frac{\partial u_i'}{\partial x_k}}+\overline{\frac{\partial u_j'}{\partial x_k}}. \tag{6}$$

Here, δ indicates the Kronecker delta and p′ denotes the fluctuating pressure.

2. Discrete Phase

2-1. Particle Phase Model

In the modeling of particle trajectories, the DPM model is used to calculate the collection efficiency and simulate the particle dispersion in the separator. The DPM model in software is based on the Euler-Lagrange method. The volume fraction of the calcium carbide slag particles selected in this study is less than 10%, and the collision between particles can be neglected. According to the Euler-Lagrange method, a single dispersed particle can be calculated.

$$\frac{du_{pi}}{dt}=F_D(u_i-u_{pi})+\frac{(r_p-r)g_i}{r_p}+F_i \tag{7}$$

where i represents the direction in which the flow parameter acts, u_{pi} is the particle velocity, the term $F_D(u_i-u_{pi})$ is drag force per unit particle mass, ρ_p is the particle density, g_i is gravitational acceleration, and F_i is an additional acceleration (force/unit particle mass) term expressed in terms of force per unit mass. For spherical particles, drag force is given as

$$F_D=\frac{18\nu}{\rho_p d_p^2}\frac{C_D Re}{24}, \tag{8}$$

where d_p is the particle diameter and R_e is the relative Reynolds number defined by

$$R_e=\frac{\rho d_p|u_p-u|}{n}. \tag{9}$$

In Fluent, the drag coefficient is given as

$$C_D=a_1+\frac{a_2}{R_{e_p}}+\frac{a_3}{R_{e_p}^2}, \tag{10}$$

where a_1, a_2, and a_3 are constants and dynamic viscosity of the fluid is 2.0e-05 Kg/m-s.

2-2. Simulation of Particle Diameter Distribution

The Rosin-Rammler distribution equation is the most commonly used function to apply particle diameter distribution. This function can discretize the particle size range into size groups, which is used in this study to simulate the particle diameter distribution of

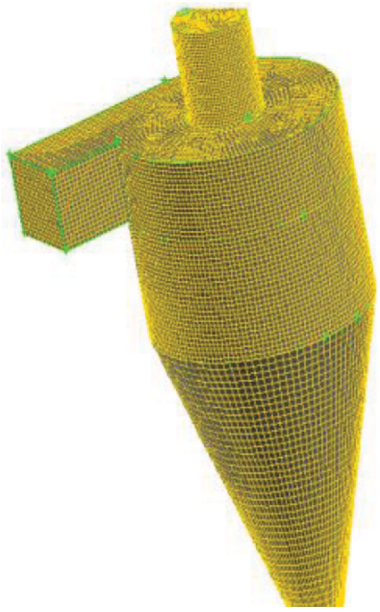

Fig. 3. Grid representation of the cyclone.

carbide slag particles. The R-R distribution function equation is described as follows:

$$G = 1 - e^{-kd_p^n} \quad (11)$$

where n is the index, k is the coefficient, and G is the cumulative weight of dust percentage.

3. Mesh Generation

The quality of CFD meshes is very critical to the numerical simulation results and it has direct impact on the accuracy of simulation results [24]. Therefore, to improve the mesh quality, the flow pattern of the separator was discretized by hexahedral grids. The grid generation software Gambit was used for discretizing the flow pattern model of cyclone separators. The mesh distribution of the gas separator in the paper is depicted in Fig. 3. To eliminate the influence of the meshes number on the numerical simulation results, the numerical results under different mesh numbers were compared to check the grid independence. As tabulated in Table 3, the simulation results of the different grid models are presented. When the number of grids was the largest or the least, the difference in results was less than 10%. This indicates that mesh independence can be obtained using a mesh with the least number of grids. However, considering the calculation time and other uncertainties, the grid with a number of 254,346 was selected for numerical simulation.

4. Boundary Condition

In this study, the inlet of the gas cyclone was set to the velocity Inlet. The continuous phase adopts the normal temperature air,

Table 3. Grid independence

Grids	Static pressure drop/Pa	Total pressure drop/Pa	Collection efficiency[a]/%
144,768	1,194	1,087	83.93
254,346	1,226	1,129	84.16
345,567	1,282	1,176	81.12
Difference (%)[b]	6.8	7.5	3.3

[a]The collection efficiency was calculated by using calcium carbide slag (particle diameter ranges from 0.01-15 μm)
[b]The proportion difference between the largest and the least grid

the viscosity is 1.8×10^{-5} kg/(m·s), the density is 1.225 kg/m^2, the air velocity is 17 m/s, the hydraulic diameter is 50 mm, the turbulence intensity is 3.1%. For the continuous phase, since the normal gradient at the outlet of the cyclone is 0, its state is a fully developed flow state, so the outlet boundary condition is set to free outflow. For the dispersed phase, the entrance speed of solid phase is the same as that of continuous phase, and only the bounce and deposition are considered when the particles move to the inner wall of the cyclone, so the inner wall is set to "reflect". Carbide slag powder with density 2,234 kg/m^3 is added from the entrance of the separator, and the Rosin-Rammler distribution is used to simulate the particle diameter distribution, the minimum particle diameter is set to 0.01 μm, and the maximum particle diameter is set to 15 μm. The boundary condition of the exhaust is set as "escape" and the dust outlet is set as "trap".

5. Solution Procedure

In the setting of solution controls, SIMPLEC coupled method was adopted for the pressure-velocity coupling; the PRESTO! pressure interpolation scheme was taken for pressure term; for momentum equations QUICK scheme was taken for spatial discretization of the advection terms. The first-order upwind scheme was used for the Reynolds stress and the second-order upwind scheme was used for the turbulent dissipation rate.

RESULTS AND DISCUSSION

1. Validation of the Numerical Results

The accuracy of the CFD models can be evaluated by comparing experimental data with predicted counterpart. The cyclone in this study is a modified cyclone separator with slotted vortex finder, which is different in structure from the traditional cyclones used in previous studies. In reality, it is very difficult to measure the velocity distribution of flow field in cyclones due to the limited experimental conditions. Therefore, to validate the above model, the experimental pressure drops were compared with simulation

Table 4. Comparison of the simulated and measured pressure drops

Slot length	0	0.2e	0.3De	0.4De	0.5De	0.6De
Numerical	1228.50	1091.20	961.00	927.60	846.40	799.50
Experimental	1220.00	1076.67	933.34	890.00	886.67	830.00
Difference (%)	0.10	0.13	2.9	4.2	4.5	3.7

results.

As shown in Table 4, the numerical results are compared with the experimental counterpart. The relative errors between experimental data and model are less than 5%, suggesting that the used CFD method is well-suited for simulating the flow field of the separator.

2. Study of Gas Flow Pattern

2-1. Comparison of the Velocity Fields in Vortex Finders

The tangential velocity and the axial velocity profiles at z=−0.04 mm in different vortex finders are plotted in Figs. 4 and 5, respectively. The figures indicate that the axial velocity and the tangential velocity in the different slotted vortex finders have axial symmetry. However, the velocity distributions in the traditional vortex finder show bad axis-symmetrical distribution. Apparently, the slotted vortex finder has an effect on the gas flow pattern in the vortex finders.

Higher tangential velocity of the flow field in the vortex finder results in higher swirling velocity of the gas flow, and the high-speed rotating flow field can bring a large amount of energy loss [25]. Fig. 4 indicates that the tangential velocity reaches the highest point near the wall and the lowest point at the center. The tangential velocity in the slotted vortex finder is significantly reduced compared with that in the traditional vortex finder. When the slot length or width of the vortex finder increases from 0.2De to 0.6De, the tangential velocity decreases. Moreover, extensive studies have shown that the reduction of the tangential velocity in the vortex finder decreases the friction between the airflow and the inner wall, thereby reducing the energy loss in the vortex finder [26,27]. Therefore, the modification of the vortex finder can reduce the tangential velocity of the gas stream in the vortex finder, and thus reduce the pressure drop of cyclone separator.

As illustrated in Fig. 5, the maximum of the upward flow of the axial velocity approaches gradually to the geometric center of the vortex finder. For the traditional vortex finder, the value of the axial velocity at the center of the flow field is positive, so there is a down-flow in the inner region. The down-flow will increase the stream resistance in the vortex finder and hence increase the pressure drop of cyclone separator [21]. Furthermore, from Fig. 5 we can also see that the axial velocity at the center is negative in the slotted vortex

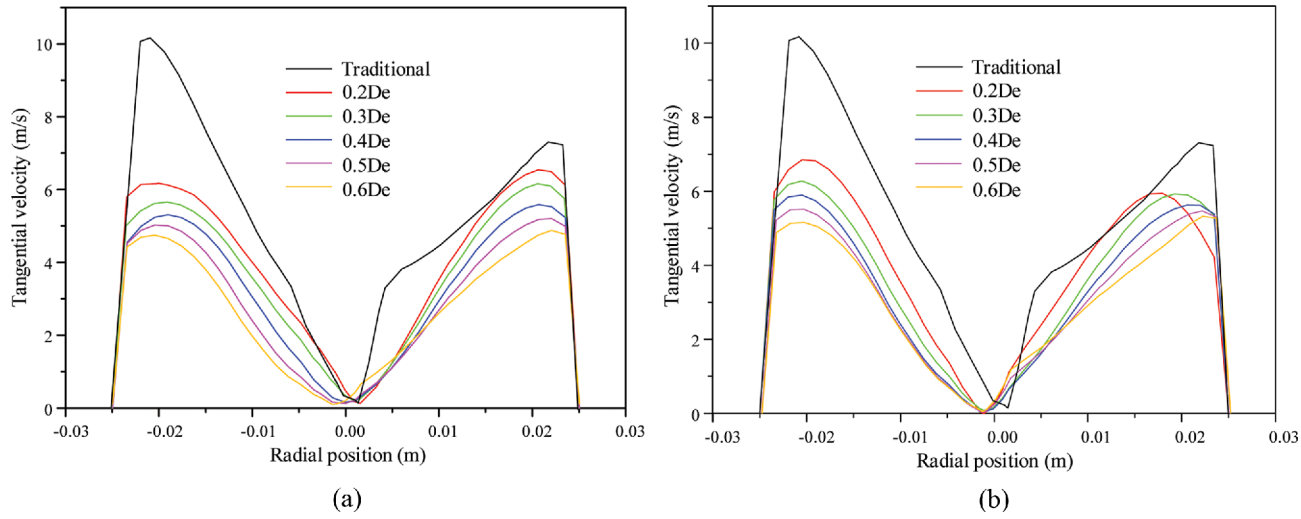

Fig. 4. The tangential velocity distributions of cyclones at z=−0.04 mm (slot length (a) and slot width (b)).

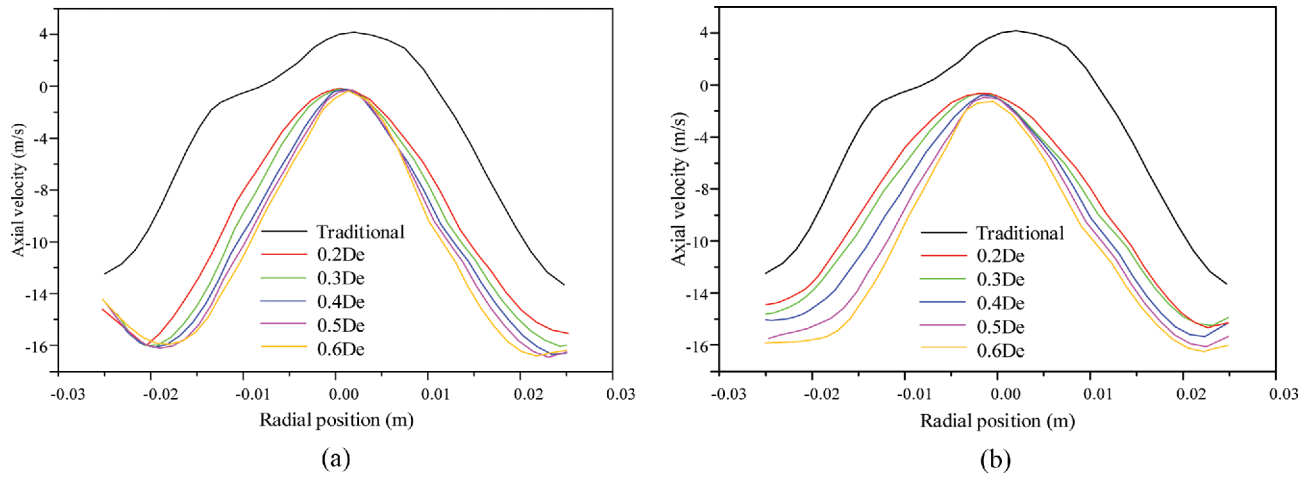

Fig. 5. The axial velocity distributions of cyclones at z=−0.04 mm (slot length (a) and slot width (b)).

finders, which shows that the down-flow in the inner region disappears. The disappearance of the down-flow makes the distribution of flow pattern in the vortex finder more uniform and reduces the stream resistance. Therefore the energy loss is reduced. In addition, some differences can be found on the axial velocity in different vortex finders. With the length and width of the slot increases, the axial velocity is reduced slightly.

2-2. Comparison of the Velocity Fields in Cyclone Chambers

The tangential velocity and the axial velocity profiles at z=0.105 mm in different cyclone chambers are plotted in Figs. 6 and 7, respectively. The profiles indicate that the swirling flow in the cyclone chambers exhibit a Rankine type vortex. The Rankine type vortex includes an inner forced vortex and an outer free vortex. Besides, the axial and tangential velocity profiles in the separator chambers show axis-symmetrical distribution.

The tangential velocity is the dominant factor of the gas flow pattern in cyclone chambers, because that can create the centrifugal force which significantly affects the separation of particles. Centrifugal force increases with the tangential velocity and thereby results in larger separation efficiency [5]. Fig. 6 shows that the tangential velocity in the inner vortex of the Rankine vortex increases with radius until it reaches a highest point, and then reduces with radius in the outer vortex. For the traditional cyclone, the tangential velocity in the cyclone body is larger than that in the corresponding parts of modified separators. The maximal value of the tangential velocity is 3.1 times that of entrance velocity and the minimal value of the tangential velocity in the outer region is 0.7 times that of the entrance velocity. For the modified separators, the maximal value of the tangential velocity is about 2.6 times that of the inlet velocity and the minimal value of the tangential velocity that of entrance velocity is 0.7 times. Moreover, the maximal tangential velocity in the outer vortex slightly decreases as the slot length and width increase, so the particles will saw a lower centrifugal force, which leads to a slightly lower separation efficiency. Fig. 6 also indicates that

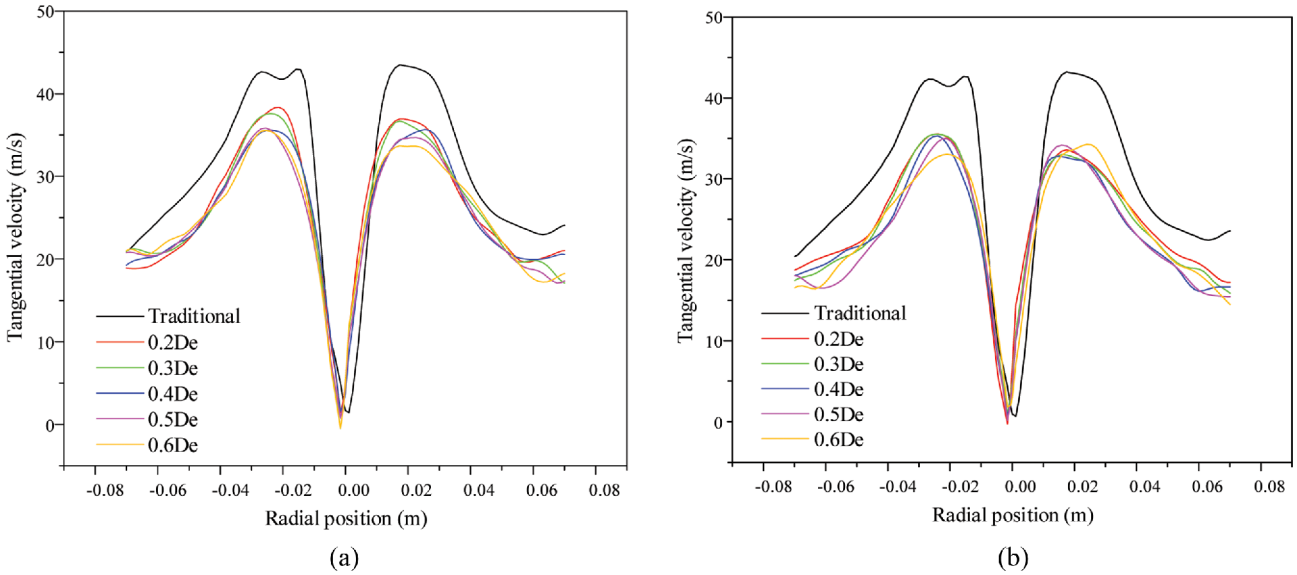

Fig. 6. The tangential velocity distributions of separators at z=0.105 mm (slot length (a) and slot width (b)).

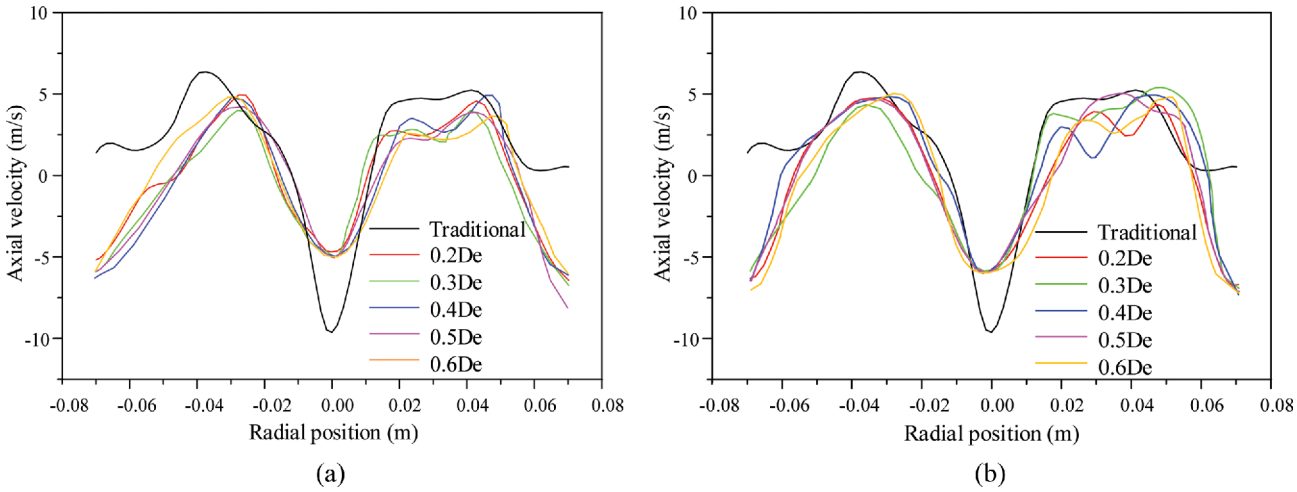

Fig. 7. The axial velocity distributions of separators at z=0.105 mm (slot length (a) and slot width (b)).

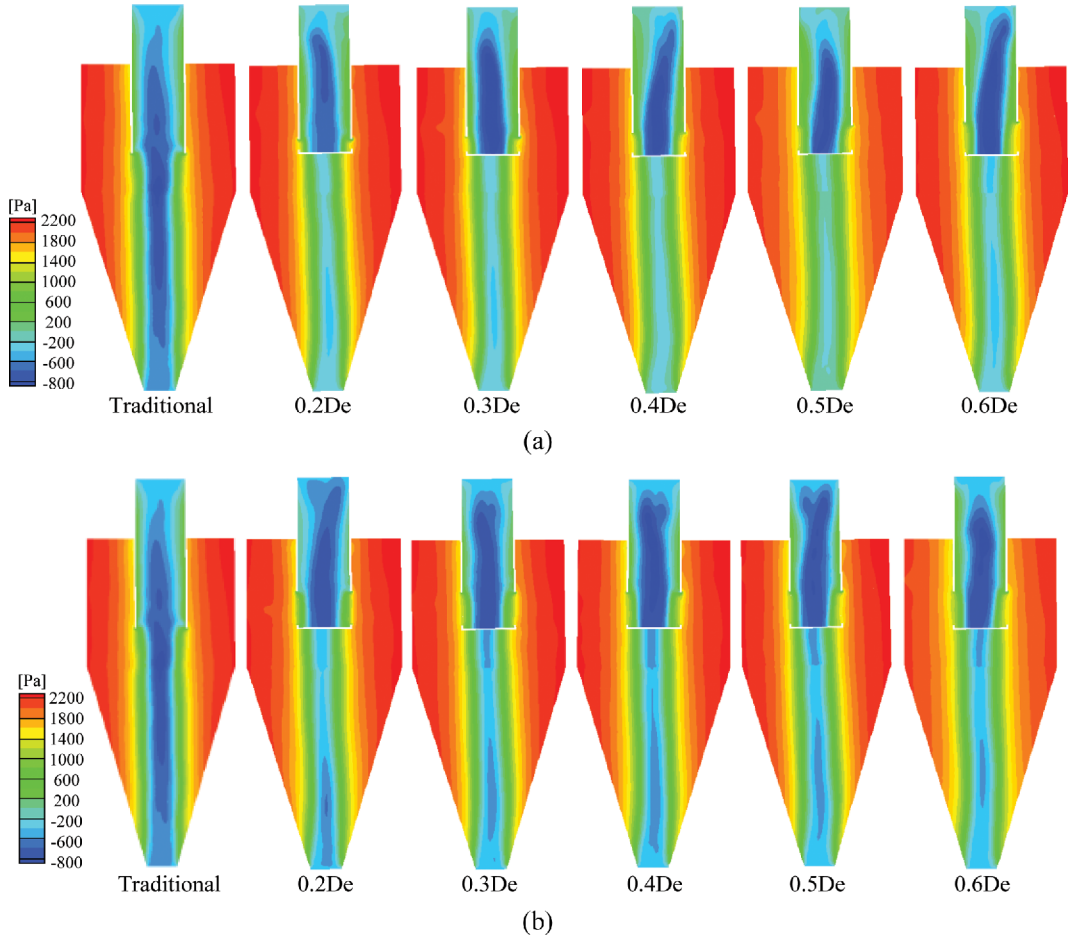

Fig. 8. Contours of static pressure of cyclones at y=0 cross-section (slot length (a) and slot width (b)).

the tangential velocity distributions in the quasi forced region for the five modified separators are nearly identical.

The axial velocity of flow field makes particles move towards the top or bottom of the separator and it is an important component that influences the performance of separator [20]. As can be seen in Fig. 7, the axial velocity distributions show that there are two flow streams. One is upward flow region and the second is downward flow region. Besides, the axial velocity distribution have the W-shaped profiles for all separators. In all cases, the highest axial velocity occurs in the radial range of 0.02 to 0.45. For the modified separators, although the change of vortex finder affect the flow field, the axial velocity profiles still exhibit a symmetrical feature. There are no obvious differences in the axial velocity distributions for these modified separators. Because the axial velocity distributions are nearly the identical, the average residence time of particles is almost the identical.

Figs. 6 and 7 also show that the tangential velocity and axial velocity in the traditional cyclone chamber is larger than that in the modified separators. This is because the axial velocity in slotted vortex finder is reduced, implying that the volume flow rate at the outlet of the vortex finder is decreased. Under the same conditions, the modified separators discharge less gas from the outlet than the traditional separator. Therefore the tangential velocity and the axial velocity of flow field in cyclone chamber decrease.

3. Pressure Distribution

Cyclone separator is an equipment that transfers the pressure energy to the dynamic energy accompanied by energy losses. Figs. 8 and 9 show the comparison of the pressure distributions between the traditional separator and modified separators. The pressure fields are primarily the same and share the same distribution features as the quasi free vortex and quasi forced vortex. In all separators, the static pressure first reduces gradually and then dramatically from the outer vortex to the inner vortex, and a negative pressure area caused by the high swirling velocity exists in the quasi forced vortex. Moreover, the gas enter and flow through the vortex finder to the outside rapidly and cause the negative pressure under and inside the vortex finder. The impact of the slot length on the static pressure is similar to that of the slot width, the maxima of static pressure near the inner wall reduce with increasing slot length and width, which indicates that less pressure potential energy converts into kinetic energy. In addition, it is obvious that the static pressure in the outer vortex slightly decreases as the slot length and width increase. Since when they increase, the total area of the slot on the vortex finder is therefore increased, leading to the increase of the volume flow rate at the outlet of the vortex finder. As a consequence, the static pressure in cyclone chamber eventually decreases.

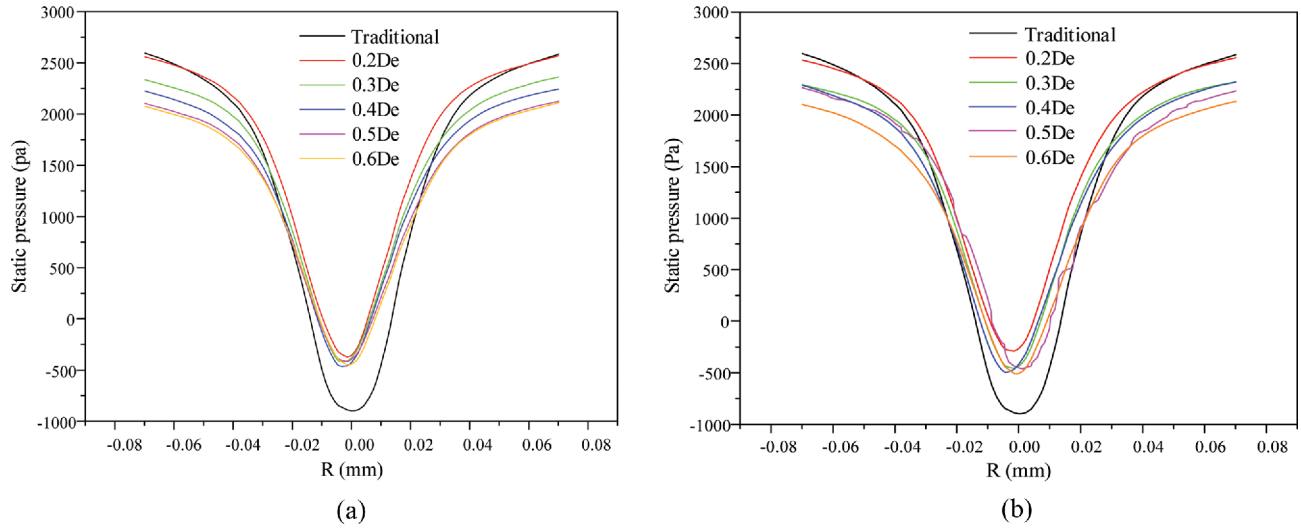

Fig. 9. The static pressure distributions of cyclones at z=0.105 mm (slot length (a) and slot width (b)).

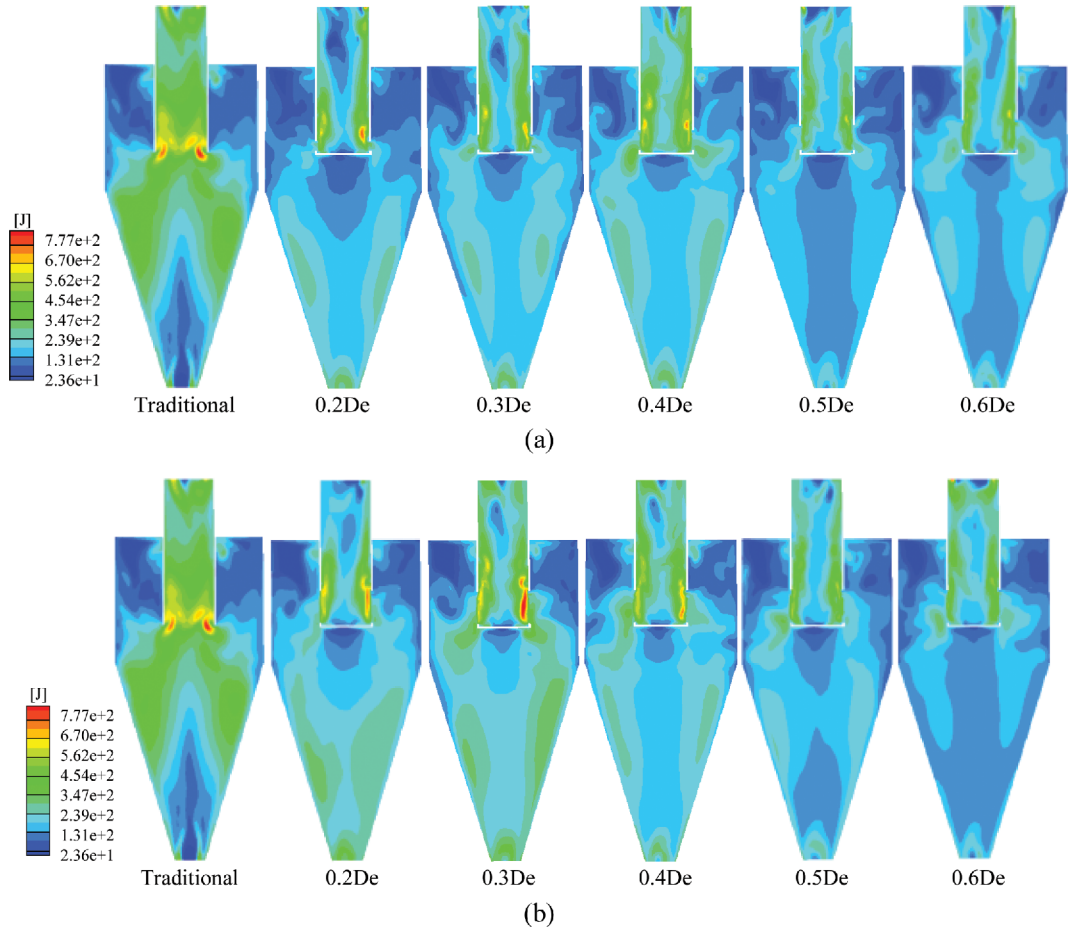

Fig. 10. Contours of turbulence intensity of cyclones at y=0 cross-section (slot length (a) and slot width (b)).

4. Turbulence Intensity

Turbulence intensity is a very important component, and influences the performance of the separator directly [22]. Fig. 10 presents the turbulence intensity contours in different cyclones. The modification of the vortex finder not only changes the turbulence intensity contours in the vortex finder, but also changes the turbulence intensity distribution in the separation chamber.

For the traditional cyclone, the maximal value of turbulence intensity occurs at the bottom of the vortex finder, and the minimal value occurs at the dust outlet. It can be showed that the most

intensive turbulence appears at the bottom of the vortex finder while the flow field is comparatively steady at the dust outlet. The maximum turbulence intensity at the bottom of the vortex finder may cause the short-circuit flow because it can drag the particles near the bottom to the inlet of the vortex finder. For the modified cyclones, the maximal value of turbulence intensity occurs near the slot, the minimum turbulent intensity occurs at the bottom of the slotted vortex finder. The turbulence intensity near the bottom of the slotted vortex finder is significantly lower than that at the corresponding part of the traditional vortex finder. This shows that the short-circuit flow is reduced. On the other hand, the turbulence intensity in the vortex finder has little changes with the reduction of the slot length and width. The turbulence energy in the cyclone chamber reduces slightly when the slot length and width increase. Pei et al. [21] reported that the decrease of the turbulence intensity in the quasi free vortex will improve the collection performance. Comparing to the traditional separator, the turbulence intensity in the quasi free vortex of modified cyclones is much lower and thereby increases the collection efficiency.

5. Particle Trajectory

5-1. Particles of the Same Particle Size Inside Cyclones with Different Vortex Finders

Fig. 11 shows a comparison of the trajectories of two particles with 1 μm diameter in different cyclones. In details, the two particles first enter the cyclone body through the inlet and rotate down with the tangential gas. For the traditional cyclone, one particle moves downward along the quasi free vortex in the separation chamber and is captured by the dust hopper, the other particle flows into the inner upward flow and discharges from the vortex finder, resulting in a strong short-circuit flow [28,29]. For the modified cyclones, when the slot length is 0.2De or 0.3De, there is no short-circuit flow in the separator chamber. However, When the slot length is >0.3De, the short-circuit flow is observed. The reason might be that as the length of the slot increases, the slot will gradually approach the inlet of the cyclone. Then, the particles from the inlet are more likely to enter the vortex finder from the slot. As a result, the separation efficiency decreases. When the slot width is >0.2De, the short-circuit flow appears due to the increase of slot area. It can be concluded that with the length and width of the slot increase, the separation efficiency of the modified separator decreases.

5-2. Particles of Different Particle Size Inside Cyclones with Different Vortex Finders

As shown in Fig. 12, particles with diameters of 0.01 to 15 μm are considered to analyze the trajectories of different particles in different separators, which are added from the same location of the inlet. Most large particles move downstream in the outer region along the quasi free vortex near the wall. Some small particles move upstream in the quasi forced vortex. Compared to the traditional separator, fewer particles discharge from the slotted vortex finder of the modified cyclone separator when the slot length and width equals to 0.2De. In this case, the collection efficiency of the new cyclone is higher than that of the traditional one. As the length and width of the slot increase, the number of particles discharges from the outlet of the vortex finder increases. Therefore, the sepa-

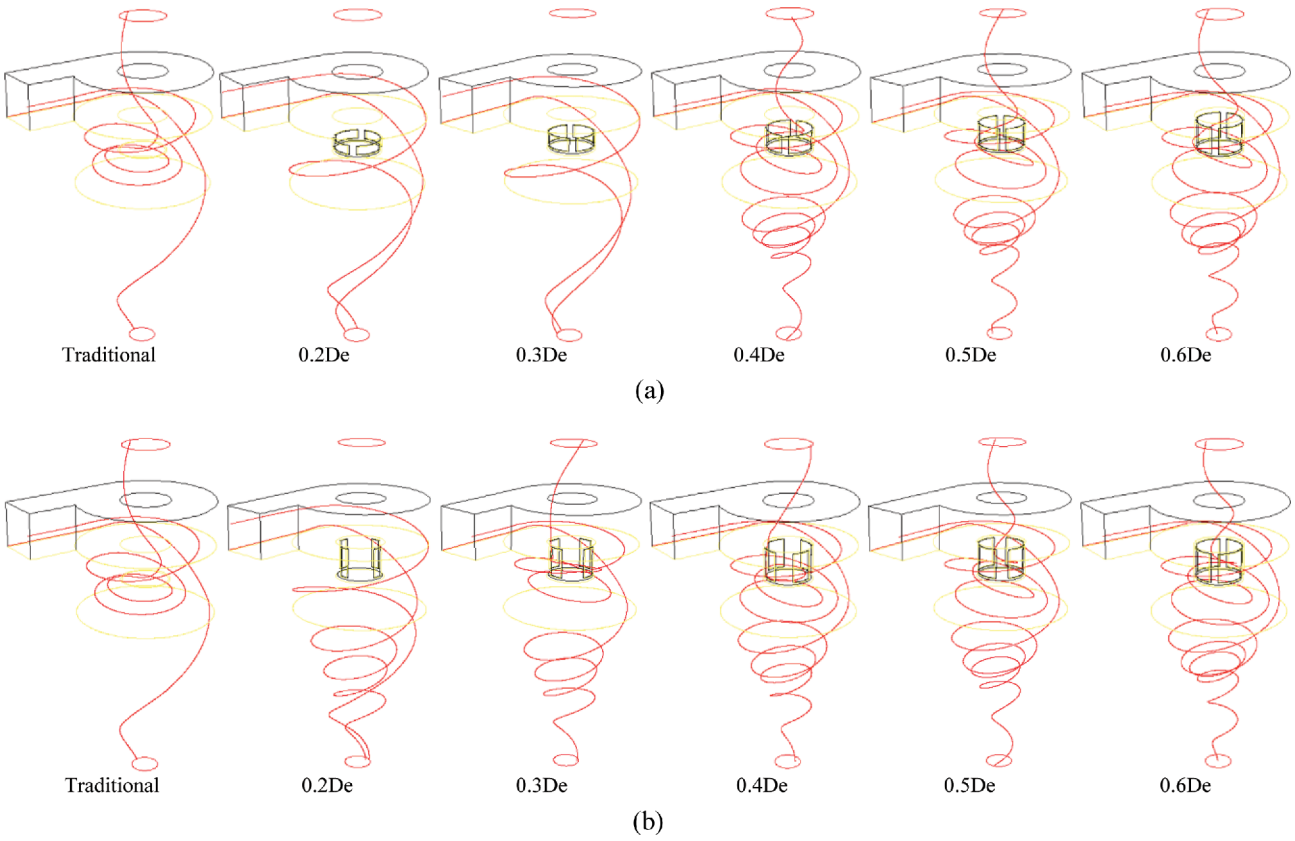

Fig. 11. Particle trajectory of 1 μm particles inside cyclones with vortex finders (slot length (a) and slot width (b)).

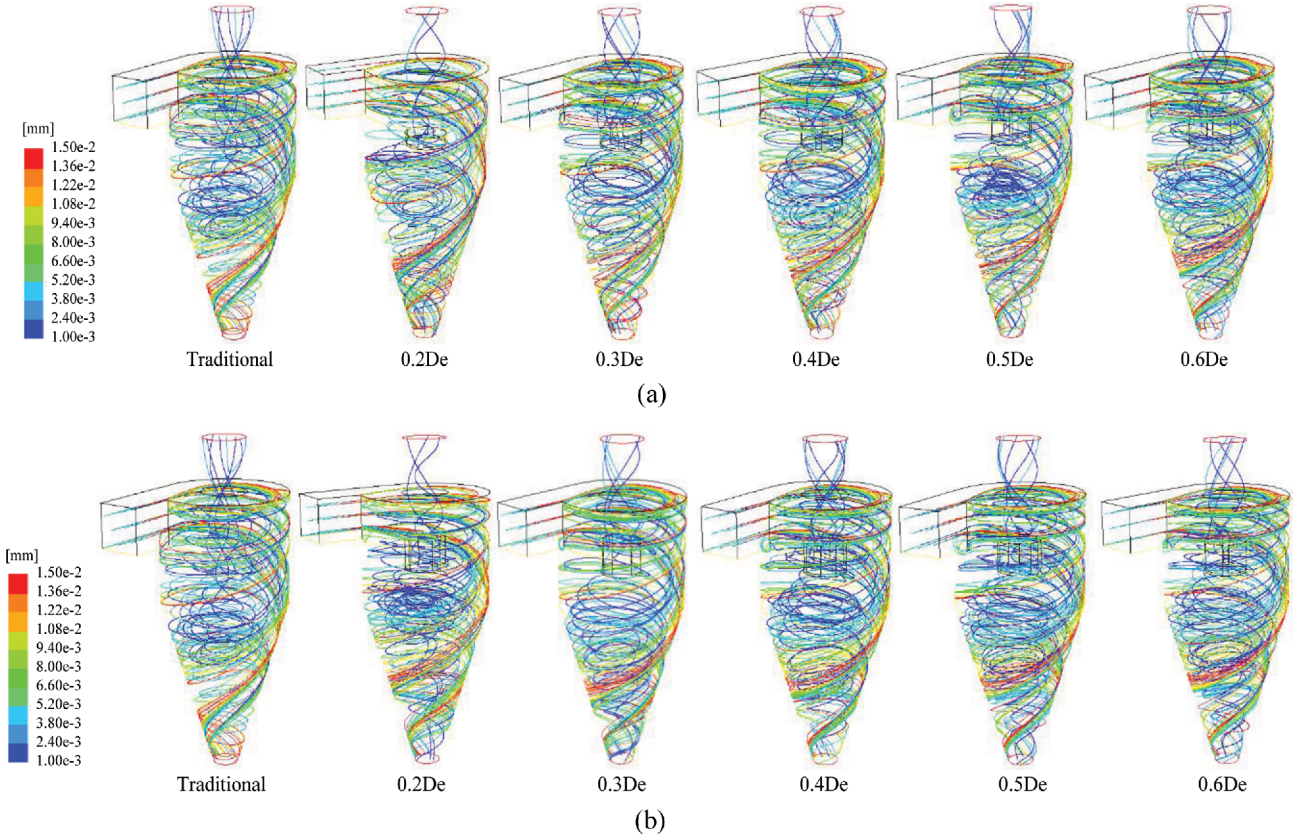

Fig. 12. Particle trajectory of 0.01 to 15 μm particles inside cyclones with vortex finders (slot length (a) and slot width (b)).

Table 5. Separation efficiencies in different slot lengths compared with experimental and numerical results

Slot length	Separation efficiency/%		Percentage increase[a]/%
	Numerical	Experimental	
0[b]	86.21	85.75	-
0.2De	91.72	91.26	5.51
0.3De	83.45	83.53	−2.22
0.4De	82.76	82.52	−3.23
0.5De	82.76	81.22	−4.53
0.6De	82.07	81.17	−4.58

[a]Percentage increase in experimental separation efficiency of new cyclones with regard to the experimental efficiency of traditional separator.
[b]The collection efficiency of traditional cyclone separator.

Table 6. Separation efficiencies in different slot lengths compared with experimental and numerical results

Slot width	Separation efficiency/%		Percentage increase/%
	Numerical	Experimental	
0	84.21	85.74	-
0.2De	88.97	90.78	5.04
0.3De	84.42	84.14	−1.40
0.4De	83.45	83.05	−2.69
0.5De	82.76	82.59	−3.15
0.6De	80.69	80.41	−5.33

ration efficiency of the modified separator decreases with the length and width of the slot increase.

6. Separation Efficiency

To analyze the experimental separation efficiency, number based calculations are not applicable to the experimental data, which are calculated by weight. The separation efficiencies from numerical simulation are obtained by the number of particles. The influence of slotted vortex finder on the separation efficiency of the separator are shown in Tables 5 and 6.

From Tables 5 and 6, we can find that the numerical results are compared with the experimental data and a good agreement is obtained. The collection efficiency of one modified cyclone is larger than that of the traditional cyclone. However, the effect of slot length or width on the efficiency are not all positive. When the slot length is 0.2De, the efficiency has a largest increase (5.51%). When the slot length and width are >0.2De, the efficiency of the new separators are lower than that of the traditional one. Besides, the efficiency of the new separator decreases as the slot length and width increase. One of the main reasons is that the slot area of the vortex finder increases as the increase of the slot length or width, leading to the increase of the probability of short-circuit of particles.

7. Pressure Drop

The pressure drop is also an important component that affects the performance of the separator directly. It mainly includes energy

Table 7. Pressure drop in different slot lengths compared with experimental and numerical data

Slot length	Pressure drop/Pa		Magnitude decrease[a]/Pa
	Numerical	Experimental	
0[b]	1,228.50	1,220.00	-
0.2De	1,091.20	1,076.67	143.33
0.3De	961.00	933.34	286.66
0.4De	927.60	890.00	330.00
0.5De	846.40	866.67	353.33
0.6De	799.50	830.00	390.00

[a]Amount decrease in experimental pressure drop of new cyclones with regard to the experimental pressure drop of traditional separator.
[b]The pressure drop of traditional cyclone.

Table 8. Pressure drop in different slot widths compared with experimental and numerical data

Slot width	Pressure drop/Pa		Magnitude decrease/%
	Numerical	Experimental	
0	1,228.52	1,220.41	-
0.2De	1,049.10	1,056.67	163.74
0.3De	950.10	936.67	283.74
0.4De	917.60	890.00	330.41
0.5De	899.20	886.67	333.74
0.6De	866.70	873.33	347.08

losses in the vortex finder and inlet and fluid swirling losses. Therefore, the pressure drop of cyclone separators should be as small as possible [30]. Cyclone pressure drops with respect to the slot length and width of vortex finder are tabulated in Tables 7 and 8.

As shown in Tables 7 and 8, the pressure drops decrease about 143.33-390.00 Pa under different slot length and width, and a good agreement can be obtained between the CFD and experimental data. For the pressure drop of cyclones with slotted vortex finders, this modification results in decreased pressure drops compared to the traditional cyclone. It can be revealed that the pressure drops of the new separators are always lower than that of the traditional separator. Besides, the pressure drop reduces sharply with the increases of the slot length and width from 0.2De to 0.6De. Comparing to the traditional separator, the pressure drop can be reduced by up to 390 Pa when the slot length is 0.6De. When the slot width equals to 0.6De, the pressure drop can be reduced by up to 347.08 Pa. One of the main reasons is that the swirling velocity of the flow field in the vortex finder reduces with increasing the slot length and width, resulting in reducing the energy loss in the vortex finder.

8. Uncertainty Analysis

From Section 2, there are system errors of different degrees in experimental system, and the error is relatively larger for some test points. A variety of factors have been implicated to contribute to the errors of the experiment. Two major factors are shown as follows:

1) The limited accuracy of the measuring instruments. When the instruments being used are not very accurate in the experiment, such as the laser particle size analyzer (range 0.2 μm to 500 μm with an accuracy of ±3%), this will cause errors in the measurement results.

2) The errors in measuring particle mass. The calcium carbide slag particles may adhere to the inner wall of the cyclone chamber and the dust collector during each experiment, which will result in inaccuracy of the separation efficiency.

To minimize the errors and obtain the accurate results, the values of the pressure drop and separation efficiency were measured three times. Before the experiment, each part of the experimental system was checked carefully, and the certain amount of calcium carbide slag particles were added to minimize the errors in measuring particle mass. To quantify the error associated with experimental data for cyclone performance, error bars are plotted on Fig. 13, which represent the standard errors for the separation efficiency and pressure drop.

As shown in Fig. 13, the predicted results reveal reasonable agreement with the experimental data. Specifically, the tendency of the efficiency and pressure drop curves is approximately identical. With these results, the potential of the RSM model to simulate flows in

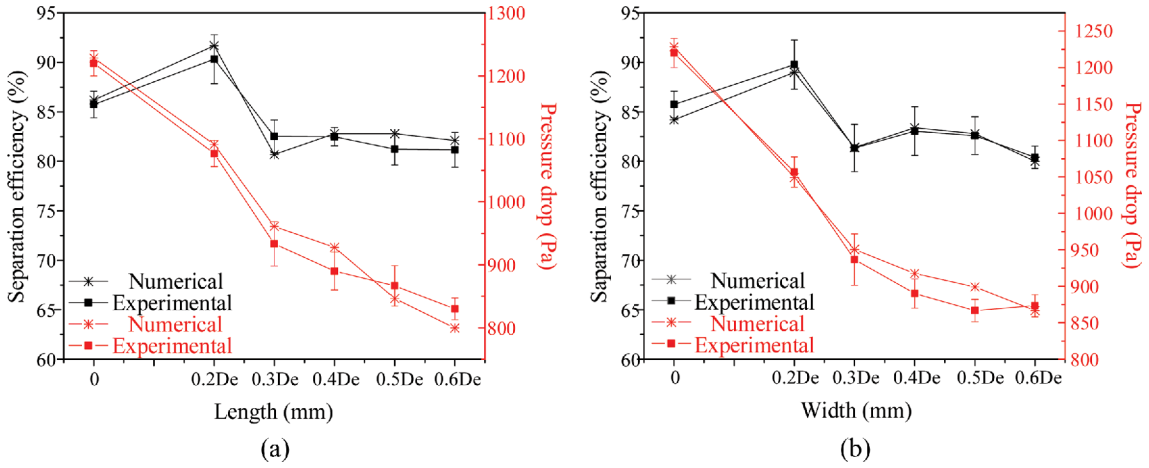

Fig. 13. Effect of slotted vortex finder on performance of cyclones (slot length (a) and slot width (b)).

a cyclone separator has been distinctly demonstrated.

CONCLUSIONS

The impact of the slotted vortex finder on the performance of different cyclones was investigated by means of CFD technique based on Reynolds stress model and experiments. The CFD data for pressure drop and separation efficiency were compared with the experimental results, revealing that the CFD technique can predict the performance of the separator. Based on the obtained numerical and experimental results, the following conclusions were drawn:

1. The slotted vortex finder can reduce the friction between the gas stream and the inner wall of the vortex finder and suppress the generation of downward flow, hence decrease the energy loss. However, the slotted vortex finder can reduce the tangential velocity in the separator chamber, and the particles will experience a lower tangential velocity, leading to a slightly lower collection efficiency.

2. The slotted vortex finder can decrease the turbulence intensity at the bottom of vortex finder and the outer region of separator chamber. Therefore, the short-circuit flow at the bottom of the vortex finder reduces and the collection efficiency increases.

3. With the length and width of the slot increase, the slot will gradually approach the inlet of the cyclone, resulting in more short-circuit flow. As a consequence, the collection performance of the modified separator diminishes.

4. The influence of slotted vortex finder on the separation efficiency is not all positive. When the slot length is 0.2De, the separation efficiency increases by 5.51%. When the slot width is 0.2De, the separation efficiency increases by 5.04%. However, when the slot length and width is >0.2De, the collection efficiency of the new separator is lower than that of the traditional one.

5. The pressure drops of the new separators are all lower than that of the traditional one. The maximal decrease of the pressure drop is 390.00 Pa when the slot length is 0.6De. When the crucial problem is the collection efficiency, the most economic condition is that there is a larger increase of the collection efficiency (5.51%) with a smaller decrease of the pressure drop (143.33 Pa) when the slot length is 0.2De.

ACKNOWLEDGEMENTS

This research is supported by the Shihezi University Key Research Youth Program of Application Foundation (No. 2015ZRKXYQ04) and the National Natural Science Foundation of China (No. 51264034).

REFERENCES

1. Y. Hiraiwa, T. Oshitari, K. Fukui, T. Yamamoto and H. Yoshida, *Sep. Purif. Technol.*, **118**, 670 (2013).
2. A. C. Hoffmann and L. E. Stein, *Gas cyclones and swirl tubes: principles, design and operation*, 2nd Ed., Springer, Berlin (2008).
3. K. S. Lim, H. S. Kim and K. W. Lee, *J. Aerosol Sci.*, **35**, 743 (2004).
4. F. Tan, I. Karagoz and A. Avci, *Chem. Eng. Commun.*, **203**, 1216 (2016).
5. R. Arman, S. Mehrzad, F. Meisam and E. Reza, *Chem. Eng. Process.*, **47**, 128 (2008).
6. S. E. Rafiee and M. M. Sadeghiazad, *Aerospace Sci. Technol.*, **63**, 110 (2017).
7. G. Jolius, T. G. Chuah, A. Fakhru' l-Razi and S. Y. Thomas, *Chem. Eng. Process.*, **44**, 7 (2005).
8. W. D. Griffiths and F. Boysan, *J. Aerosol Sci.*, **27**, 281 (1996).
9. A. J. Hoekstra, J. J. Derksen and H. E. A. Van Den Akker, *Chem. Eng. Sci.*, **54**, 2055 (1999).
10. M. D. Slack, R. O. Prasada, A. Bakkera and F. Boysana, *Chem. Eng. Res. Design*, **78**, 1098 (2000).
11. L. Z. Wang, J. M. Feng, X. Gao and X. Y. Penga, *Chem. Eng. Res. Design*, **117**, 394 (2017).
12. Q. Li, W. W. Xu, J. J. Wang and Y. H. Jin, *Sep. Purif. Technol.*, **141**, 53 (2015).
13. H. M. El-Batsh, *Appl. Math. Model.*, **37**, 5286 (2013).
14. J. H. Chen and X. Liu, *Sep. Purif. Technol.*, **73**, 100 (2010).
15. E. Khairy and L. Chris, *Comput. Fluids*, **51**, 48 (2011).
16. L. S. Brar, R. P. Sharma and R. Dwivedi, *Part. Sci. Technol.*, **33**, 34 (2015).
17. Y. Zhu and K. W. Lee, *J. Aerosol Sci.*, **30**, 1303 (1999).
18. S. E. Rafiee and M. M. Sadeghiazad, *J. Marine Sci. Appl.*, **15**, 388 (2016).
19. X. Gao, J. F. Chen, J. M. Feng and X. Y. Peng, *Comput. Fluids*, **92**, 45 (2014).
20. P. Farzad, H. H. Seyyed, A. Goodarz and E. Khairy, *Sep. Purif. Technol.*, **187**, 1 (2017).
21. B. B. Pei, L. Yang, K. J. Dong, Y. C. Jiang, X. S. Du and B. Wang, *Powder Technol.*, **313**, 135 (2017).
22. S. E. Rafiee and M. M. Sadeghiazad, *J. Marine Sci. Appl.*, **15**, 157 (2016).
23. S. B. Lakhbir and K. Amit, *CFD simulations of cyclone separators with different diameters*, 2015 1st international conference on futuristic trends on computational anslysis and knowledge management, 180 (2015).
24. J. A. Feng, X. Q. Tang and W. B. Wang, *J. Shehezi Univ.: Natural Sci.*, **35**, 52 (2017).
25. J. J. Wang, L. Z. Wang and C. W. Liu, *Chin. J. Process Eng.*, **5**, 251 (2005).
26. A. C. Hoffmann, L. E. Stein and P. Bradshaw, *Appl. Mech. Rev.*, **56**, B28 (2003).
27. Y. H. Jin, G. Q. Ji, Q. Y. Cao and J. J. Wang, *J. China Univ. Petroleum*, **32**, 109 (2008).
28. B. Wang and A. B. Yu, *Chem. Eng. J.*, **135**, 33 (2008).
29. Y. X. Su, A. G. Zheng and B. T. Zhao, *Powder Technol.*, **210**, 293 (2011).
30. G. B. Sakura and A. Y. T. Leung, *Powder Technol.*, **286**, 488 (2015).